THE ASTROPHYSICAL JOURNAL, 328:256–264, 1988 May 1

HYDRODYNAMIC MODELING OF AN X-RAY FLARE ON PROXIMA CENTAURI OBSERVED BY THE *EINSTEIN* TELESCOPE

F. REALE, G. PERES, AND S. SERIO[1]
Osservatorio Astronomico di Palermo
R. ROSNER
Harvard-Smithsonian Center for Astrophysics
AND
J. H. M. M. SCHMITT
Max-Planck-Institut für Extraterrestrische Physik
Received 1987 June 26; accepted 1987 September 28

ABSTRACT

We present hydrodynamic numerical calculations of a flare which occurred on Proxima Centauri and was observed by the *Einstein* satellite on 1980 August 20 at 12:50 UT. The numerical code is a version of a hydrodynamic model for magnetically confined plasmas, which has previously been extensively tested and applied to solar flares and has now been extended to the study of more general stellar environments. To the best of our knowledge, this is the first attempt to perform a detailed hydrodynamic modeling of a stellar flare.

We compare the X-ray light curves observed in various energy channels of the imaging proportional counter with the predictions of the hydrodynamic model. By analogy with solar loop flares, the stellar flare is assumed to be caused by a heating pulse deposited inside a semicircular magnetic loop confining stellar coronal plasma which is initially static. By adjusting the parameters characterizing both the initial loop atmosphere and the flare impulsive heating rate, we obtain good agreement between computed and observed X-ray light curves. Our results are consistent with the stellar flare being caused by the rapid (~ 700 s) dissipation of 5.9×10^{31} ergs, within a magnetic loop structure whose semilength is $L = 7 \times 10^9$ cm and cross-sectional radius is $r = 7.3 \times 10^8$ cm. This loop is slightly smaller than the Proxima Centauri stellar radius, but much larger than its initial coronal pressure scale height; compared to compact solar flare loops, it appears to be larger, but of similar L/r ratio.

Our results provide evidence that flares on late-type stars can be described by a hydrodynamic model with a relatively simple geometry, similar to solar compact flares. Since energy release in stellar flares may exceed that of solar flares by orders of magnitude, the use of our model can help to constrain physical quantities (such as, for instance, coronal magnetic fields) presently not directly observable, under conditions widely different than those prevailing on the Sun.

Subject headings: hydromagnetics — stars: flare — stars: individual (Proxima Cen) — X-rays: bursts

I. INTRODUCTION

Recently, much effort has been devoted to the study of solar flares by hydrodynamic models using energy, momentum, and mass-conservation equations to compute the evolution of flaring plasma confined in magnetic flux tubes (Nagai 1980; Peres *et al.* 1982; Pallavicini *et al.* 1983; Cheng *et al.* 1983; Doschek *et al.* 1983; MacNeice *et al.* 1984; MacNeice 1986*a*, *b*; Cheng, Karpen, and Doschek 1985; Nagai and Emslie 1984; Fisher, Canfield, and McClymont 1985*a*, *b*, *c*; Peres *et al.* 1987). These models generally concern compact loop flares, i.e., flares occurring in closed loops, where the magnetic structure suffers little or no disruption during the event (Pallavicini, Serio, and Vaiana 1977). In particular, it has been shown that a hydrodynamic model using simple assumptions for the energy deposition mechanism can reproduce fairly well the evolution of observed X-ray emission in high-ionization lines over a wide range of excitation energies during a solar flare (Peres *et al.* 1987).

Since the discovery that most stars have solarlike coronae (e.g., Vaiana *et al.* 1981), hydrostatic coronal models have been applied with some success (Giampapa *et al.* 1985; Landini *et al.* 1985; Stern, Antiochos, and Harnden 1986; Schmitt *et al.* 1985). Here we present an extension of hydrodynamic modeling to the stellar environment and, in particular, to a specific stellar flare observed by the *Einstein* satellite. We consider the event observed on Proxima Centauri on 1980 August 20 at 12:50 UT by the *Einstein* imaging proportional counter (IPC). This event has been described previously by Haisch *et al.* (1983) and Haisch (1983).

Proxima Centauri, the star nearest to the Sun ($d = 1.3$ pc), is a late-type star with spectral type dM5e, radius $\sim \frac{1}{7} R_\odot$ (Pettersen 1980), and mass $\sim 0.2\ M_\odot$ (Allen 1973). It is a well-known example of an optical flare star and shows substantial X-ray emission, even in quiet conditions (Haisch *et al.* 1978; Haisch *et al.* 1980; Haisch *et al.* 1981; Haisch *et al.* 1983; Haisch and Linsky 1980).

Due to the lack of spatial resolution, stellar X-ray observations can provide no direct information about the geometry and dimension of the flaring region. However, by considering both the dynamical nature of the event and a simple model for the decay phase of the flare, one can infer that the flare occurred in a closed region of dimension $\sim 10^9$–10^{10} cm (Haisch 1983). The purpose of our hydrodynamic calculations is to provide a more complete model with which more detailed

[1] Istituto per le Applicazioni Interdisciplinarie della Fisica, Palermo.

estimates of the flare geometry and parameters can be evaluated.

In this paper, we first describe the available observations and the data reduction procedures (§ II) and illustrate the highlights of the hydrodynamic code (§ III). We then derive the physical and geometrical parameters necessary for the calculations and compare the results with the observations (§ IV). Our results are discussed in § V. We discuss the accuracy of the numerical calculations in the Appendix.

II. OBSERVATIONS AND DATA ANALYSIS

The flare was observed between 12:50 and 14:40 UT on 1980 August 20 at X-ray wavelengths by the *Einstein* IPC and in the *UV* by the *IUE* satellite (Haisch *et al.* 1983); due to the lack of time resolution in this latter set of data, we use only *Einstein* data in our analysis.

The IPC had a field of view of $\sim 1°$, with a spatial resolution of $\sim 1'$. Its energy sensitivity lies in the range $\sim$0.04–14.0 keV, dropping off sharply at $\sim$0.2 keV at low energies and at $\sim$4.0 keV at high energies, with a spectral resolution $\Delta E/E \sim 1$ at 1 keV. The temporal resolution of the observations was 63 μs. Our analysis differs from the previous analysis of this event (Haisch *et al.* 1983) because we use the much improved REV-1B version of the data-processing software (Harnden, Fabricant, and Schwartz 1984), which represents the final IPC calibration.

Details of the X-ray observation are presented in Table 1. As an aside, we note that the instrument gain remained substantially constant, with changes $\lesssim 0.5\%$ within the entire observation period. The data used for comparison with model predictions are count rates in each IPC energy channel in the standard processing cell of 3′ radius around the centroid of the X-ray source. For each energy band, we subtracted the average count rate in the preflare phase in order to remove the contributions of quiet coronal emission and the background.

The observation is essentially continuous for over 20 ks; however, three large sections (from $t = 5653$ to 8520 s, from $t = 11{,}305$ to 11,500 s, and from $t = 16{,}958$ to 19,702 s, reckoning the time from 1980 August 20, 10:27 UT, when the X-ray observation started) show anomalous background because of spacecraft "day," etc. Hence, four periods of continuous "clean" coverage are available. Luckily, the entire flare and pre-flare emission was observed during these periods, its rise and decay phases clearly discernable. We thus have precise information on the onset of the event and the preflare state.

The peak count rate (without subtraction of the quiet coronal emission component preceding the flare and of the background component) reaches 3.3 counts s^{-1} in channels 1–15 of the IPC, i.e., $\sim$20 times higher than the preflare count rate, which is $\sim$0.17 counts s^{-1}. Using a factor to convert from IPC count into X-ray flux of 2×10^{-11} ergs cm^{-2} count^{-1}, we obtain a peak X-ray flare luminosity of $\sim 1.2 \times 10^{28}$ ergs s^{-1} and an integrated flare energy in the IPC energy band of $E_x \sim 2.1 \times 10^{31}$ ergs. Assuming an average emissivity of $P \sim 2 \times 10^{-23}$ ergs cm^3 s^{-1}, the emission measure is of the order of 10^{51} cm^{-3}. These values are consistent with the values reported by Haisch *et al.* (1983).

Figure 1*a* shows the X-ray count rate integrated in IPC channels 1–15 (corresponding to the full IPC energy band). Fits to a uniform temperature, optically thin plasma, and

TABLE 1

OBSERVATIONAL PARAMETERS OF THE PROXIMA CENTAURI FLARE ON 1980 AUGUST 20 AT 12:50 UT

IPC Sequence number	7689
Starting time of observation (UT)	1980, Aug 20, 10:27
Total observation time	20,193 s
Observation live time	17,890 s
Peak count rate[a]	3.3 s^{-1}
Preflare count rate [b]	0.17 s^{-1}
Total source counts	8925

[a] Including background, in the standard detection cell (22.5 × 22.5 pixels^2).
[b] Average count rate in the time interval from 2621 to 5653 s.

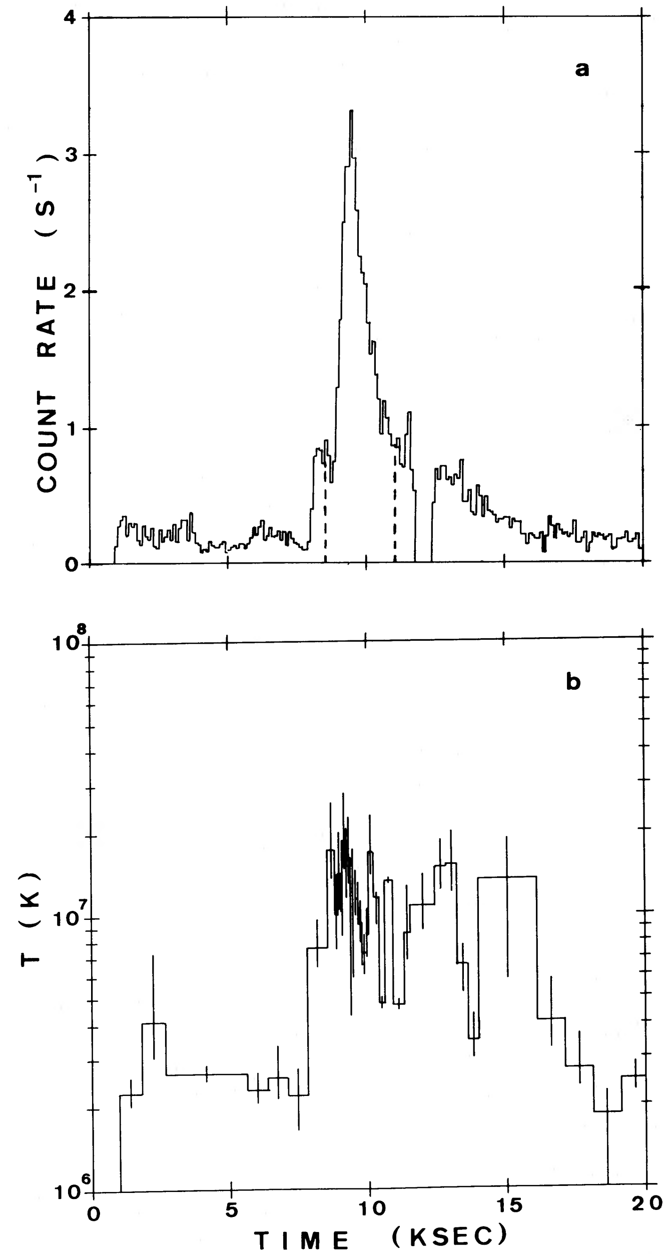

FIG. 1.—(*a*) Observed light curve in the IPC X-ray band derived from REV-1B processing (raw counts without corrections for background). The dashed vertical lines bound the time range covered by our hydrodynamic calculations. (*b*) Evolution of the best-fit temperature (single-component, see text).

assuming a Raymond and Smith (1977) spectrum, were performed on the different phases of the flare; these gave values of temperatures ranging from $T \sim 2.6 \times 10^6$ K in the quiet phase to $T \sim 2 \times 10^7$ K at the peak of the event (Fig. 1*b*). These values are to be considered as purely indicative, given the obvious limitations of single-temperature models during a highly dynamic phenomenon such as a flare.

At the very beginning of the second "clean" observation interval ($t \sim 8500$ s), an increase of the X-ray emission followed by a return to lower flux levels is detected just before the rise phase of the flare proper. We cannot ascertain whether this early activity is due to a brief flare in another region of the corona or, in close analogy to many solar flares, to some kind of precursor activity. Similarly, during the decay phase, at times later than 10,250 s, we see statistically significant enhancements of X-ray emission. This might mean that secondary events are accompanying the main flare or that other regions of the stars are flaring. Indications that energetic events are occurring in this phase can also be inferred from the temperature evolution. In either case, in order to account for multiple events or for strongly time-structured impulsive energy release, we would need to substantially increase the numbers of degrees of freedom in our calculations. Therefore, for simplicity's sake, we have limited our study to the time interval from 8500 s to $\sim$ 10,500 s, without attempting to model the enhancements at the beginning and at the end of this interval.

Inside this interval, except near the extremes, the X-ray light curve is very similar to that of typical compact solar flares, with rise and decay *e*-folding times of 500 and 1000 s, respectively. The temperature evolution is also similar to that of solar flares: its rise time is below the temporal resolution allowed by the temperature fit, while its decay time is roughly $\sim$1000 s, i.e., of the same order of magnitude as the decay time of the X-ray integrated count rate.

III. THE NUMERICAL CODE

The calculations were performed with the Palermo-Harvard hydrodynamic numerical code described by Peres *et al.* (1982), Pallavicini *et al.* (1983), Peres and Serio (1984), and Peres *et al.* (1987). This code describes the evolution of plasma confined in a semicircular rigid loop. Plasma motions and heat transport are assumed to be one-dimensional, that is, to be constrained to flow along a sufficiently strong magnetic field whose geometry is not essentially modified during the event. While this hypothesis is well founded for compact solar flares, it cannot be directly tested on a star, and its validity rests solely on the comparison of the results of the calculations with the observations, as shall be discussed below. We show that the relatively slow decay of the flare can be explained by assuming a sufficiently long and rigid closed loop (while still retaining realistic bounds on the magnetic fields); hence, the suggestion of Haisch *et al.* (1983) that the long decay time is evidence for a two-ribbon flare is not the only plausible explanation for this event.

The code solves the equations of mass and momentum conservation using explicit integration schemes and the equation of energy conservation by an implicit method (Richtmyer and Morton 1967; Roache 1976). Ionizational equilibrium is assumed, and the effects of gravity and viscosity are included in the momentum-conservation equation, together with a numerical viscosity introduced in order to treat shock effects (see Peres *et al.* 1982 for further details). In the energy equation, the Spitzer (1962) thermal conductivity is adopted, while coronal radiative losses are calculated by parameterizing the optically thin plasma radiative-cooling function as in Rosner, Tucker, and Vaiana (1978). The integration time step is continuously monitored and limited by the local radiative cooling time and by the Courant stability condition. Stability is also assured by the adoption of upwind differencing.

The assumed loop geometry is semicircular, with symmetric boundary conditions at the top; the spatial coordinate along the loop is sampled with constant logarithmic spacing in order to achieve higher resolution in the geometrically thinner chromospheric and transition regions. Calculations have been performed by adopting spatial grids of 128, 256, and 512 points (see the Appendix).

In order to match the model to the physical conditions of the Proxima Centauri atmosphere, some modifications of the treatment of the lower atmosphere with respect to the solar case (e.g., Peres *et al.* 1982) are necessary. The coronal model for the initial static loop configuration, within which the flare takes place, is matched to an empirical chromospheric model selected among those developed by Cram and Mullan (1979). In particular, we have adopted their model 6 (in agreement with the evidence for emission Balmer lines in the spectrum of Proxima Centauri), slightly adjusting the column density at $T = 9 \times 10^3$ and 10^5 K in order to match the pressure at the top of the chromosphere with that at the base of the corona. The chromospheric temperature distribution is then simply obtained by numerically integrating the hydrostatic equation. The more detailed and accurate chromosphere models of Giampapa, Worden, and Linsky (1982) for representative dM and dMe stars with well-observed Ca II K lines cannot be used for Proxima Centauri because of a lack of evidence for Ca activity. The influence of the details of the chromospheric model on the accuracy of the code is, however, minor, as discussed in the Appendix.

In our model, the minimum (or loop footpoint) temperature is $T = 2659$ K, lower than the corresponding solar temperature minimum of 4400 K; the chromospheric height is $\delta h_c \sim 140$ km. Because of a lack of stringent observational constraints on the conditions of the preflare atmosphere, the initial pressure at the top of the chromosphere is set at $p_0 = 10$ dyn cm^{-2}, a reasonable typical value (see Cram and Mullan 1979; Giampapa, Worden, and Linsky 1982). The hydrodynamic and thermodynamic equations are the same as in the solar case, except for the values of the stellar surface gravity (here $g_* = 2.7 \times 10^5$ cm s^{-2}) and stellar radius (here $R_* = 10^{10}$ cm). The relatively large value of the surface gravity, $\sim$10 times solar, implies a small coronal pressure scale height with respect to the solar case, provided that the coronal temperature is similar to the solar one ($s_p \sim 1.3 \times 10^9$ cm, with $T \sim 2.5 \times 10^6$ K).

We assume that the thermal phase of the flare is caused by a strong heat pulse superposed on a stationary heating function which, in the absence of flare-like perturbations, maintains thermal balance in the loop. In the Palermo-Harvard code, the heat pulse can be either parameterized as a function of time and field-line coordinate or computed via an explicit model, viz., via local heating due to a beam of high-energy nonthermal electrons which precipitate from the loop apex to the loop footpoints and deliver their energy and momentum to the confined plasma as they thermalize (described in Peres *et al.* 1987). Since stellar observations do not allow a choice between these models, we have chosen a parameterized heating function: a

Gaussian heat pulse centered at the top of the loop. This model is simpler than the electron-beam model and gave good results in fitting the X-ray light curves for the solar event described in Peres *et al.* (1987); furthermore, due to the high conductivity of the hot plasma, the difference between results of calculations differing in the assumed spatial distribution of the heating pulse are not appreciable in the present observational framework, provided that the heat pulse is mostly released in the coronal region of the loop. The impulsive heating term (energy deposited per unit time per unit volume) is therefore

$$Q_i(x, t) = Hf(t)g(x) , \quad (1)$$

where x is the coordinate along the loop, H is the peak value of the volumetric heating rate,

$$g(x) = \exp\left[-(x - x_0)^2/2\sigma^2\right] \quad (2)$$

is the heating distribution along x, and

$$f(t) = \begin{cases} 1 , & t_0 < t \le t_1 , \\ 0 , & t > t_1 , \end{cases} \quad (3)$$

describes the heating temporal distribution. The crucial quantities specifying the heating pulse are the heating flux,

$$F = \sqrt{\pi/2}\sigma H , \quad (4)$$

and the total deposited energy,

$$E_{\rm tot} = 2\pi r^2(t_1 - t_0)F , \quad (5)$$

where r is the cross-sectional radius of the loop (we assume σ to be significantly smaller than the loop semilength).

Finally, we note that the high plasma densities and temperatures encountered in this stellar event, when compared to the solar compact flares previously studied with this code, require better time and space resolution in the calculations and therefore more powerful computing resources. We have therefore developed a version of the Palermo-Harvard code optimized for vector-oriented computers and have run most of the computations on a CRAY-XMP/12. This new version of the code has been carefully tested against calculations performed with the previous version of the Palermo-Harvard code.

IV. THE CALCULATIONS

The goal of the calculations was to reproduce the *Einstein* observations as closely as possible. While a number of parameters determine the results of the calculations, a full exploration of the parameter space was not feasible on computational grounds nor warranted by the quality of the observations. However, the parameter space can be restricted by qualitative estimates, especially by taking advantage of our previous experience in modeling solar flares.

All calculations (summarized by models I–IV below) are characterized by the parameters of the heating function and of the preflare atmosphere (see, for example, Pallavicini *et al.* 1983). Some of these parameters (namely the duration of the heat pulse and the initial coronal pressure) are difficult to constrain, and are therefore derived by educated guesses, while others (in particular, the length of the loop, its cross section, and the heating flux pulse power) are estimated by comparing the numerical results with the observational data.

a) Initial Dimensions of the Loop

The dimensions of the model loop were derived by starting from an initial rough estimate and obtaining better estimates from the comparison of the calculations with the observations. For the starting estimate, we used dimensional analysis. As evident in Figure 1, both the X-ray emission and temperature decay times are of the order of 1000 s. As a first approximation, the global decay time can be expressed as

$$\frac{1}{\tau_{\rm obs}} = \frac{1}{\tau_{\rm cond}} + \frac{1}{\tau_{\rm rad}} , \quad (6)$$

where

$$\tau_{\rm cond} \approx \frac{3nkL^2}{\kappa T^{5/2}} \quad (7)$$

and

$$\tau_{\rm rad} \approx \frac{3kT}{nP(T)} . \quad (8)$$

In equations (6)–(8), $\tau_{\rm obs}$, $\tau_{\rm cond}$, and $\tau_{\rm rad}$ are, respectively, the observed, conductive, and radiative decay times, n is the particle number density, k is the Boltzmann constant, L is the loop semilength, κ is the thermal conductivity, T is the temperature, and $P(T)$ is the radiative losses per unit emission measure. If we assume an effective $\langle P(T)\rangle \sim 2 \times 10^{-23}$ ergs cm^3 s^{-1}, then the emission scales as

$$\mathrm{EM} = \int_V n^2\, dV \approx n^2 V \approx 2\pi n^2 \alpha^2 L^3 , \quad (9)$$

where V is the volume and α the aspect ratio of the loop, i.e., the ratio between the loop cross-sectional radius and the loop semilength.

By taking $T \sim 10^7$ K, EM $\sim 10^{51}$ cm^{-3} (as suggested by the X-ray observations), and $\alpha \sim 0.1$, we can now estimate the loop semilength,[2] obtaining $L \sim 10^{10}$ cm. This value is much larger than the initial pressure scale height, and therefore the loop is mostly empty in this first calculation. Although this loop is much larger than the one obtained by Haisch (1983) (who based his result on the assumption of equality between the radiative, conductive, and observed decay times and obtained $L \sim 2.5 \times 10^9$ cm), we shall nonetheless use it as a starting point for our optimization procedure. As we shall discuss below, the results of our hydrodynamic calculations for loop lengths shorter than 5×10^9 cm are not easily made compatible with the X-ray observations.

b) Initial Parameters of the Heating Function

An approximate knowledge of the energy liberated in the flare can be obtained from the X-ray observations and by estimating the energy radiated in other frequency bands. This procedure was adopted for the flare under study by Haisch *et al.* (1983), who found $E_{\rm tot} \sim 3.5 \times 10^{31}$ ergs. This value is subject to large uncertainties, so we shall use it only as a starting point for our iterative procedure.

Once $E_{\rm tot}$ is fixed, the heating pulse power and heating duration can no longer be chosen independently. Indirect observational clues are available for estimating the duration of the heat pulse if we are guided by the analogy between this flare and solar flares. Given the wide energy response of the IPC,

[2] Note that this initial choice of α, which is similar to that for typical solar loops, is introduced only to estimate the *initial* value of the loop semilength. We shall determine this parameter more precisely later on, showing that it represents a normalization factor for the computed X-ray emission of the coronal loop (see eq. [11] below).

TABLE 2

PARAMETERS OF THE NUMERICAL MODELS

Model (1)	I (2)	II (3)	III (4)	IV (5)
Coronal base pressure (dyn cm^{-2})	10	10	10	10
Loop semilength (10^9 cm)	10	7	5	7
Impulsive heat flux (10^{10} ergs cm^{-2} s^{-1})[a]	1.25	1.25	1.25	2.5
Heating time (s)	700	700	700	700
Loop aspect ratio	0.14	0.17	0.20	0.10
Loop cross section (10^{18} cm^2)	6.3	4.2	3.3	1.7
Total input energy (10^{31} ergs)	11.0	7.4	5.8	5.9
Peak temperature (10^7 K)	4.2	3.9	3.5	4.5
Peak plasma density (10^{10} cm^{-3})[b]	5	7	10	13
Peak plasma pressure (10^3 dyn cm^{-2})[b]	0.3	0.5	0.7	1.0

[a] In one semiloop.

[b] Average above 2×10^7 cm from the loop base.

which extends down to 0.04 keV, the X-ray light curve is fundamentally governed by the evolution of the emission measure (and therefore of the average density for a flare occurring within a confined volume), but is relatively insensitive to the average plasma temperature. Since coronal temperatures can increase only while excess heating is being supplied, the duration of the temperature rise phase can be taken as an indication of the duration of the heating pulse. The emission measure, on the other hand, can continue to increase long after heat deposition has stopped, because of chromospheric ablation and expansion. Consequently, the heating term in our calculations has to be switched off well before the emission peak is observed. Using an emission measure rise time of 1000 s, estimated on the basis of the IPC light curve (Fig. 1), we have fixed the duration of the heating phase as $t_1 - t_0 = 700$ s; the subsequent comparison of the results of the calculations with the observations supports this choice. The peak volumetric heating rate H to use in our calculations (eq. [1]) can now be estimated from the total flare energy and the dimensions of the loop:

$$H = \sqrt{\frac{2}{\pi}} \frac{E_{tot}}{2\pi\sigma\alpha^2 L^2(t_1 - t_0)} . \tag{10}$$

c) *Iterative Determination of the Flare Loop Characteristics*

Knowing the full spectral response function of the IPC, we can obtain a synthetic X-ray light curve from the computed values of density and temperature:

$$C(t) = \frac{\alpha^2 L^2}{4d^2} \int_0^L n^2(x, t) G[T(x, t)] dx , \tag{11}$$

where $C(t)$ is the predicted count rate, d is the distance to Proxima Centauri, and $G(T)$ is the plasma emissivity at temperature T folded through the instrumental response.

The time of onset of the impulsive heating term, t_0, can be determined, together with the aspect ratio, α, by properly shifting and scaling the computed light curve to best fit the observed one.

The results of the initial trial calculation, using the above estimated values of the loop length and impulsive heating parameters (model I; see Table 2, col. [2]), are illustrated by the thin solid line in Figure 2. While the rise phase is satisfactorily reproduced (apart from the precursor phase, which we do not attempt to model), it is immediately apparent that the decay of the X-ray luminosity of the computed flare is much slower than suggested by the observations; for this reason, computations were stopped to save computer time. Since the decay time typically decreases with the loop length because of the shorter conductive time, we deduce that the loop length should be reduced to improve the agreement between model and data.

Two more calculations were then performed, using $L = 7 \times 10^9$ cm (model II; see Table 2, Col. [3]) and $L = 5 \times 10^9$ cm (model III; see Table 2, col. [4]), respectively. The smallest of these values for the loop semilength is still more than twice as large as Haisch's (1983) value. For models II and III we assumed the same total impulsive heating as in model I, but concentrated in a region half as extended as before; consequently, we doubled the impulsive heating peak

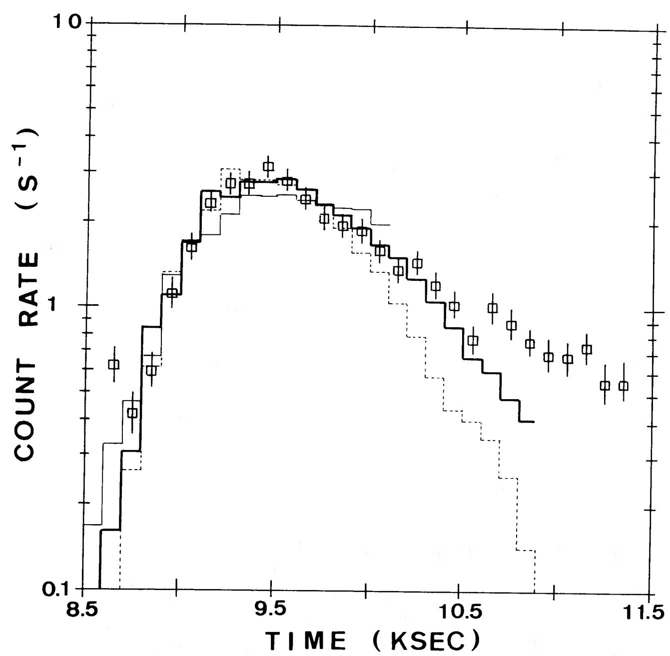

FIG. 2.—Comparison between the flare light curve observed by the IPC X-ray band (*squares*) and the computed light curves for flare loops of semilength $L = 10^{10}$ cm (*thin solid line*), $L = 7 \times 10^9$ cm (*heavy line*), and $L = 5 \times 10^9$ cm (*dashed line*) and subjected to a heating flux pulse of $F = 1.25 \times 10^{10}$ ergs cm^{-2} s^{-1} lasting 700 s (models, I, II, and III, respectively). Note that the starting time of each calculation (with respect to 1980 August 20, 10:27 UT) and the normalization of the computed light curve (i.e., the aspect ratio of the model loop) are derived by a best fit to the observed light curve.

intensity H. As evident from Figure 2, model II shows the best agreement with the observations. It is obvious that further adjustments of the loop length would be unwarranted due to uncertainties in the data and in the model. However, the moderate spectral resolution of the IPC does allow us to further constrain the impulsive heating flux, as described below.

d) Determination of the Impulsive Heating Flux

The detected photons are distributed over 15 pulse height channels in the IPC, so that a spectral analysis can be carried out to obtain further constraints on the thermal parameters of the flare. In fact, due to the large uncertainty in the value of total flare energy used to determine the value of the heat flux, we still have some freedom to change this parameter. Based on our previous experience in solar flare calculations, if we increase the heat flux in our calculations, we expect an increase in the amount of plasma at higher temperatures (see also Jackimiec *et al.* 1986). We have extended the technique used by Schmitt *et al.* (1985) in their analysis of static loop models of the corona of Procyon to compare the evolution of the IPC spectral distribution during the Proxima Centauri flare with the results of our calculations. From the calculated distribution of density and temperature of the loop plasma, we determined the temperature distribution of the differential emission measure during selected time intervals; we then computed the emission of the entire loop using a Raymond-Smith (1977) thermal spectrum, and folded it through the IPC spectral response function at the appropriate instrument gain and with the appropriate corrections to derive the distribution of predicted counts in each IPC channel.

To ascertain the dependence of our model flare on the impulsive heating flux, we have performed a further calculation, using $L = 7 \times 10^9$ cm as in model II, but doubling the heating flux (model IV; Table 2, col. [5]). As is discussed in the Appendix, in this case we had also to double the number of grid points in our numerical model, so as to properly handle the increased particle density in the evaporating plasma.

In Figure 3 we compare the evolution of the calculated (models II and IV) X-ray emission in the whole IPC band and in three selected groupings of adjacent IPC channels: 1–4, 5–6, and 7–10, corresponding to the energy ranges 0.04–0.81, 0.81–1.38, and 1.38–3.50 keV, respectively (we do not use channels 11–15, corresponding to energies higher than 3.5 keV, because of poor count statistics). While the quality of the fit to the integrated IPC light curve does not differ appreciably for these calculations (Fig. 3*a*), in model IV the computed X-ray emission in the harder channels is higher than in model II and closer to the observations. As before, further adjustments are not warranted by the quality of the data or by the accuracy of the model.

V. DISCUSSION OF THE RESULTS

As is apparent from the relative behavior of models I–IV, our hydrodynamic calculations are sensitive to parameters characterizing the geometry of the flaring loop and the impulsive heat deposition causing the flare. In particular, we find that model II and, especially, model IV reproduce the observed IPC light curves and spectral distribution of this flare fairly well. Assuming that the flare indeed did occur in a rigid loop-like structure, our calculations can therefore be used to derive features of the flare morphology which cannot be obtained by direct observations, as well as features of the energy budget of the event.

We have compared the results of three calculations differing only in the adopted loop length (models I, II, and III), and, taking advantage of the strong dependence of the decay times on the loop length, we have concluded that the Proxima Centauri flare of 1980 August 20 at 12:50 UT most likely occurred in a coronal loop with semilength $L \sim 7 \times 10^9$ cm. As implied by the decay of the X-ray light curves in models I and III, the semilength of the corresponding loops (10^{10} and 5×10^9 cm, respectively) can be taken as the extremes of the confidence interval of our determination of the semilength of the flaring loop. As an aside, we note that the length of the flaring structure could be somewhat shorter than 7×10^9 cm if some heating deposition continues during the decay phase of the event (e.g., Peres *et al.* 1987). We have ignored this possibility in our approach in order to avoid introducing additional model parameters without the benefit of a significant gain in physical insight.

We have then used the computed X-ray spectral distribution to ascertain that the initial choice for the impulsive heating flux causing the flare could be improved to account for the spectral distribution of the observed counts. We were thus led to a revised model (model IV), which is characterized by the same loop semilength as determined above ($L \sim 7 \times 10^9$ cm) but by a maximum impulsive heating flux twice as large as in the previous model (i.e., $F = 2.5 \times 10^{10}$ ergs cm^{-2} s^{-1}). This final model also gives the best overall fits to the time evolution of the spectrally resolved count rates.

Using the parameters for model IV, the total energy dissipated in the flare is estimated to be $E_{\text{tot}} \sim 5.9 \times 10^{31}$ ergs. This value is approximately one order of magnitude higher than in typical solar compact flares and is comparable to that of the largest solar flares; it is comfortably close to the total flare energy estimated by Haisch *et al.* (1983) by extrapolating the X-ray luminosity to the entire electromagnetic band ($E_{\text{tot}} \sim 3.5 \times 10^{31}$ ergs).

Our methodological approach has been to gain morphological information on the source by a detailed analysis of its time variability and with the use of a physical model. We have shown that this approach can, in fact, partially overcome the lack of spatial resolution in stellar observations. We show in Figure 4 (Plate 6) a conceptual synthesis of our results, comparing the model flaring loop in Proxima Centauri to a typical solar compact flare. The flare dimensions are of the same order of magnitude as the stellar radius itself. Indeed, the flare we have just studied occurs in a loop larger than typical compact solar flare loops, but comparable to the largest compact solar flare in the *Skylab* survey of limb flares by Pallavicini, Serio, and Vaiana (1977).

The observation of another flare on Proxima Centauri by *Einstein* on 1979 March 6, which showed a similar emission decay time, suggests that this configuration is not unusual (Haisch and Linsky 1980; Haisch *et al.* 1981). Regions of strong activity on Proxima Centauri are therefore similar in size to (or larger than) the regions where the largest compact solar flares occur. This suggests the presence of relatively large magnetic field structures in the atmosphere of Proxima Centauri and, by inference, of other similar late-type stars. Moreover, as is shown by the value of the loop cross section in Table 2, the aspect ratio of the Proxima Centauri flaring loop is similar to those of solar coronal loops.

The validity of the above results rests essentially on the validity of our basic assumption, i.e., that of rigid confinement. Its plausibility can be tested by considering the value of the

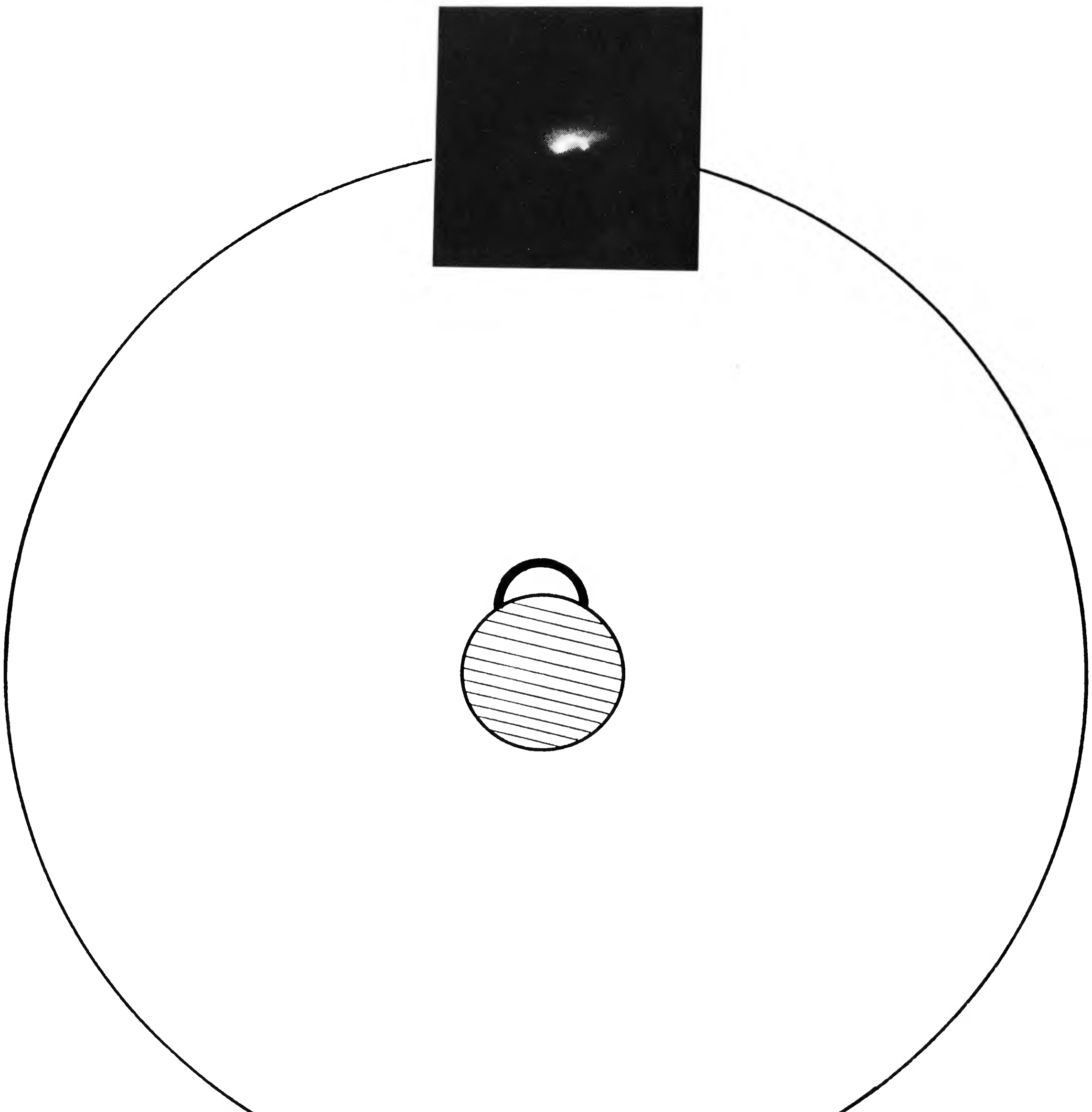

FIG. 4.—Synthesis of the Proxima Centauri flare loop geometry compared with that of a typical solar compact flare. The large circle represents the solar limb, and the shaded disk Proxima Centauri; the drawings are scaled appropriately. The "best-fit" stellar flaring loop is then compared with a typical compact solar flare observed by the S-054 X-ray telescope onboard *Skylab*, shown in the inset (adapted from Fig. 5 in Pallavicini, Serio, and Vaiana 1977).

REALE *et al.* (*see* **328**, 261)

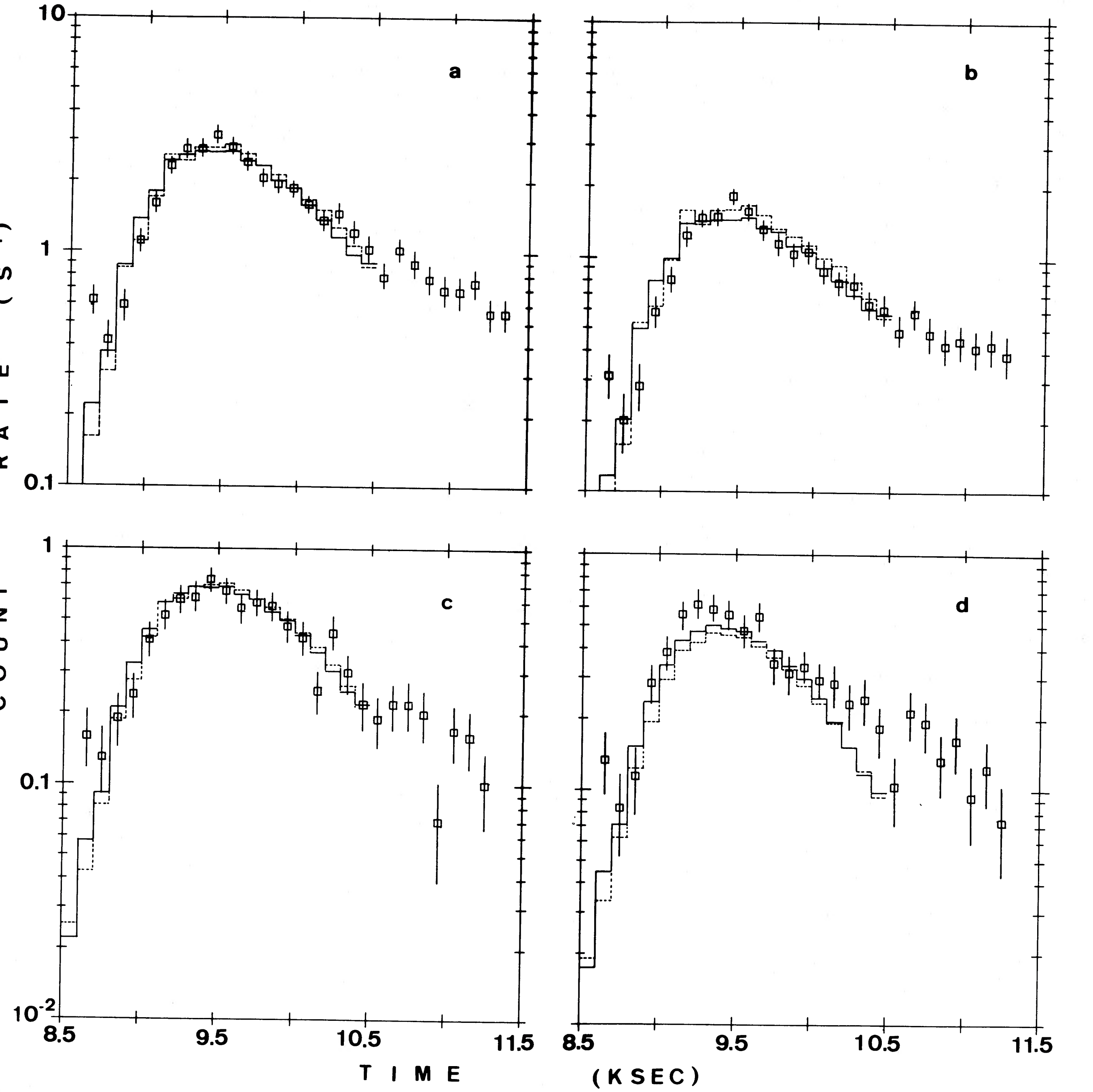

FIG. 3.—Comparison between the observed (*squares*) and computed light curves for models II (*dashed line*: impulsive energy flux $F = 1.25 \times 10^{10}$ ergs cm^{-2} s^{-1}) and IV (*solid line*: impulsive energy flux $F = 2.5 \times 10^{10}$ ergs cm^{-2} s^{-1}). The four panels show, respectively, the results for the full IPC energy band (*a*), and for the energy bands 0.04–0.81 keV (*b*), 0.81–1.38 keV (*c*), and 1.38–3.50 keV (*d*).

computed flare peak pressure as a lower limit to the confining magnetic pressure. In the case of our flare, the peak pressure is well within solar flare standards. The validity of our rigid loop assumption requires the presence of coronal magnetic fields $B > 8\pi p^{1/2} \sim 100$ G. Although this value might appear somewhat high, analogous estimates of the lower limit of the constraining magnetic fields in a sample of 25 compact solar flares observed during the *Skylab* mission (Pallavicini, Serio, and Vaiana 1977) are on average $B_{\min} \sim 50$ G, with three events with $B_{\min} > 90$ G. Even though the flaring loop in Proxima Centauri is larger than typical solar compact flare loops, the possibility that magnetic fields of ~ 100 G are present at a height $2L/\pi \sim 5 \times 10^9$ cm in the corona of Proxima Centauri appears not to be unrealistic, and the basic assumption of our model is therefore plausible.

We wish to point out, however, that the agreement between our numerical results and the observational data does not represent an absolute test for the validity of the closed loop model. This model represents a working hypothesis, following from an immediate extension of solar analysis to stellar flares. The large dimensions of the flaring region suggested by our calculations are rather puzzling, especially considering that a loop of semi-length $\sim 7 \times 10^9$ cm is ~ 4 times larger than the pressure scale height of the assumed initial static atmosphere and therefore initially quite empty over a large fraction of its volume. Thus, the possibility of adjustments in the configuration of the magnetic field when the loop is filled by the evaporating plasma cannot be ruled out. In fact, the intensity and duration of this flare were considered as prima facie evidence for a two-ribbon flare (Haisch *et al.* 1983), based on solar standards. This possibility cannot be readily excluded; although expansion cooling can reduce the decay time of an unconfined flare of comparable mean size, energy deposition during the decay phase, as a result of continuing rearrangement of the magnetic field structure, can act in the opposite direction. The balance of these two effects in two-ribbon solar flares does typically give larger decay times than for compact flares. Therefore, if the magnetic topology during the flare is subject to changes and if these changes are accompanied by further energy release, then we might expect that the mean dimensions of the flaring region are somewhat smaller than suggested by our calculations.

Our calculations appear to be perfectly adequate for a comparison with the available data; more sophisticated numerical codes, which take into account other physical effects such as loss of confinement, will not be sufficiently constrained. Only future experiments can provide better constraints. Consider, for example, chromospheric evaporation: the average plasma density in the loop increases from the very low values characterizing the initial unperturbed loop to typical solar compact flare values ($\langle n \rangle_{\rm peak} \sim 10^{11}$ cm^{-3}), with $\sim 3 \times 10^{39}$ particles brought up from the chromosphere to the corona in ~ 1000 s; this occurs at speeds up to ~ 600 km s^{-1}. Doppler-shifted X-ray lines originating in this large amount of "evaporating" plasma may be detected by the next generation of X-ray space missions and therefore could provide additional sensitive constraints to hydrodynamic flare modeling.

We wish to thank F. R. Harnden, Jr., for assistance in obtaining and analyzing the X-ray data, F. D. Seward for his invaluable criticism and comments, A. Collura, S. Sciortino, and G. S. Vaiana for useful discussions. This work was supported in part by Consiglio Nazionale delle Ricerche and Ministero Pubblica Istruzione, by a NASA *Einstein* Guest Investigator grant to Harvard University (RR), and by the Max-Planck Gesellschaft für Extraterrestrische Physik (JS).

APPENDIX

ACCURACY OF THE SPATIAL GRID AND OF THE CHROMOSPHERIC MODEL

In this Appendix, we discuss inaccuracies in the calculated count rates resulting from numerical effects. Most of the calculated X-ray emission is produced in the lower region of the corona, where the plasma is denser. This region is immediately adjacent to the transition region, where the code's spatial resolution is limited (Peres, Rosner, and Serio 1987); this resolution limitation leads to unavoidable errors in the calculation and produces perceptible noise in the computed light curves, especially in the softer energy channels. In order to ascertain and define the influence of this effect, we have performed a number of identical calculations, varying only the resolution of the code's spatial grid. In particular, we have run model I for the rising phase of the flare using grids of 128, 256, and 512 points. We have found appreciable differences between the runs with 128 and 256 points and very minor differences between runs with 256 and 512 points; in this last case, numerical noise is practically absent. To limit the computing time, we have therefore adopted a spatial grid of 256 points for models I, II, and III and have increased the grid spatial resolution to 512 points only for the final model IV. In this last case, the stronger and more impulsive heating produces more violent chromospheric "evaporation" and steeper gradients, so that higher spatial resolution is required, despite the considerable increase in computer time.

A different source of possible inaccuracy in the calculations is the chromospheric model used. We have tested its influence by comparing the results obtained for model I (using the Cram and Mullan [1979] chromospheric model) with those obtained with a rough and very different chromospheric model defined as follows: we arbitrarily scale the solar chromosphere model used in previous applications of the Palermo-Harvard hydrodynamic code to solar flares (Peres *et al.* 1987 and references therein), using the scaling laws given by Hammer (1983) for static stellar coronae. As expected, this procedure gives unrealistic results for the thermal structure of the lower atmosphere (for example, a minimum temperature of ~ 6000 K). Nonetheless, we find, upon comparing with our earlier calculations, that the overall light curve is essentially unmodified, though some differences are apparent in the X-ray spectral distribution. These differences are, however, rather minor, especially when considering the radical change in the chromosphere. Since the assumed Cram and Mullan (1979) model is physically plausible, we conclude that further improvements in the chromospheric model would not significantly improve the quality of the results, given the indeterminacy of other flare parameters and the limited accuracy of the observational data.

REFERENCES

Allen, C. W. 1973, *Astrophysical Quantities* (London: Athlone Press).
Cheng, C.-C., Karpen, J. T., and Doschek, G. A. 1985, *Ap. J.*, **286**, 787.
Cheng, C.-C., Oran, E. S., Doschek, G. A., Boris, J. P., and Mariska, J. T. 1983, *Ap. J.*, **265**, 1090.
Cram, L. E., and Mullan, D. J. 1979, *Ap. J.*, **234**, 579.
Doschek, G. A., Cheng, C.-C., Oran, E. S., Boris, J. P., and Mariska, J. T. 1983, *Ap. J.*, **265**, 1103.
Fisher, G. H., Canfield, R. C., and McClymont, A. N. 1985*a*, *Ap. J.*, **289**, 414.
———. 1985*b*, *Ap. J.*, **289**, 425.
———. 1985*c*, *Ap. J.*, **289**, 434.
Giampapa, M. S., Golub, L., Peres, G., Serio, S., and Vaiana, G. S. 1985, *Ap. J.*, **289**, 203.
Giampapa, M. S., Worden, S. P., and Linsky, J. L. 1982, *Ap. J.*, **258**, 740.
Haisch, B. M. 1983, in *Activity in Red Dwarf Stars*, ed. M. Rodonó and P. B. Byrne (Dordrecht: Reidel), p. 255.
Haisch, B. M., and Linsky, J. L. 1980, *Ap. J.* (*Letters*), **236**, L33.
Haisch, B. M., Linsky, J. L., Bornmann, P. L., Stencel, R. E., Antiochos, S. K., Golub, L., and Vaiana, G. S. 1983, *Ap. J.*, **267**, 280.
Haisch, B. M., Linsky, J. L., Hanrden, F. R., Jr., Rosner, R., Seward, F. D., and Vaiana, G. S. 1980, *Ap. J.* (*Letters*), **242**, L99.
Haisch, B. M., Linsky, J. L., Slee, O. B., Hearn, D. R., Walker, A. R., Rydgren, A. E., and Nicolson, J. D. 1978, *Ap. J.* (*Letters*), **225**, L35.
Haisch, B. M., *et al.* 1981, *Ap. J.*, **245**, 1009.
Hammer, R. 1983, *Ap. J.*, **280**, 780.

Harnden, F. R., Jr., Fabricant, D. G., and Schwartz, J. 1984, *Smithsonian Ap. Obs. Spec. Rept.*, No. 393.
Jakimiec, J., Sylwester, B., Sylwester, J., Mewe, R., Peres, G., Serio, S., and Schrijver, J. 1986, *Adv. Space Res.*, **6**, in press.
Landini, M., Monsignori-Fossi, B. C., Paresce, F., and Stern, R. A. 1985, *Ap. J.*, **289**, 709.
MacNeice, P. 1986*a*, *Solar Phys.*, **90**, 357.
———. 1986*b*, *Solar Phys.*, **103**, 47.
MacNeice, P., McWhirter, R. W. P., Spicer, D. S., and Burgess, A. 1984, *Solar Phys.*, **90**, 357.
Nagai, F. 1980, *Solar Phys.*, **68**, 351.
Nagai, F., and Emslie, A. G. 1984, *Ap. J.*, **279**, 896.
Pallavicini, R., Peres, G., Serio, S., Vaiana, G. S., Acton, L., Leibacher, J., and Rosner, R. 1983, *Ap. J.*, **270**, 270.
Pallavicini, R., Serio, S., and Vaiana, G. S. 1977, *Ap. J.*, **216**, 108.
Peres, G., Reale, F., Serio, S., and Pallavicini, R. 1987, *Ap. J.*, **312**, 895.
Peres, G., Rosner, R., Serio, S., and Vaiana, G. S. 1982, *Ap. J.*, **252**, 791.
Peres, G., and Serio, S. 1984, *Mem. Soc. Astr. Italiana*, **55**, 749.
Peres, G., Rosner, R., and Serio, S. 1987, *Nuovo Cimento B*, **99B**, 29.
Pettersen, B. R. 1980, *Astr. Ap.*, **82**, 53.
Raymond, J. C., and Smith, B. W. 1977, *Ap. J. Suppl.*, **35**, 419.
Richtmyer, R. D., and Morton, K. W. 1967, *Finite Difference Methods for Initial Value Problems* (New York: Wiley Interscience).
Roache, P. J. 1976, *Computational Fluid Dynamics* (Albuquerque: Hermosa).
Rosner, R., Tucker, W. H., and Vaiana, G. S. 1978, *Ap. J.*, **220**, 643.
Schmitt, J. H., Harnden, F. R., Jr., Peres, G., Rosner, R., and Serio, S. 1985, *Ap. J.*, **288**, 751.
Spitzer, L. 1962, *The Physics of Fully Ionized Gases* (New York: Interscience).
Stern, R. A., Antiochos, S. K., and Harnden, F. R., Jr. 1986, *Ap. J.*, **305**, 417.
Vaiana, G. S., *et al.* 1981, *Ap. J.*, **245**, 163.

GIOVANNI PERES, FABIO REALE, and SALVATORE SERIO: Osservatorio Astronomico, Piazza del Parlamento 1, 90134 Palermo, Italy

ROBERT ROSNER: Department of Astronomy and Astrophysics and Enrico Fermi Institute, University of Chicago, Chicago, IL 60637

JURGEN H. M. M. SCHMITT: Max-Planck-Institut für Extraterrestrische Physik, D-8046 Garching bei Munchen, Federal Republic of Germany